Infragravity rip current pulsations

Jamie H. MacMahan
Oceanography Department, Naval Postgraduate School, Monterey, California, USA

Ad J. H. M. Reniers
Civil Engineering and Geosciences, Delft University of Technology, Delft, Netherlands

Edward B. Thornton and Tim P. Stanton
Oceanography Department, Naval Postgraduate School, Monterey, California, USA

Received 28 July 2003; revised 6 October 2003; accepted 18 November 2003; published 31 January 2004.

[1] The origins of rip current pulsations within the infragravity frequency band (0.004–0.04 Hz) are determined from measurements made with arrays of colocated pressure and velocity sensors deployed on a beach with persistent rip current channels. The observations indicate significant energy in cross-shore infragravity velocities that varies spatially in the alongshore due to the presence of rip channels. Infragravity velocities are smaller within the rip channel than on the shore-connected shoal owing to differences in water depth. Rip current pulsations at infragravity frequencies are linked to standing infragravity motions but not to the ponding and subsequent release of water by wave group pumping. *INDEX TERMS:* 4546 Oceanography: Physical: Nearshore processes; 4560 Oceanography: Physical: Surface waves and tides (1255); 4599 Oceanography: Physical: General or miscellaneous; *KEYWORDS:* rip current, nearshore circulation, infragravity, waves, surf zone

Citation: MacMahan, J. H., A. J. H. M. Reniers, E. B. Thornton, and T. P. Stanton (2004), Infragravity rip current pulsations, *J. Geophys. Res.*, *109*, C01033, doi:10.1029/2003JC002068.

1. Introduction

[2] Rip currents are strong (up to 2 m s^{-1}) jet-like seaward-directed flows that originate within the surf zone. There have been few field measurements of topographically controlled rip currents owing to the extreme difficulty deploying instruments within the rip current channels, which tend to migrate alongshore. Rip current pulsations (temporal modulations of the rip current velocities) generally have been attributed to wave groups, but complete spatial and temporal field measurements have not been available to evaluate this relationship.

[3] Observations of currents within rip channels demonstrate pulsations on the wave group timescales (25–250 s) [*Shepard et al.*, 1941; *Shepard and Inman*, 1950; *Sonu*, 1972; *Aagaard et al.*, 1997; *Brander and Short*, 2001]. However, these observations were not accompanied by simultaneous measurements of offshore waves nor of waves alongshore of the rip channel, precluding the investigations of relationships between rip currents and the approaching wave groups.

[4] Additional lower-frequency motions of nongravity waves associated with rip current shear instabilities [*Smith and Largier*, 1995; *Brander and Short*, 2001; *Haller and Dalrymple*, 2001] and wave group–induced vortices [*Reniers et al.*, 2004] may also contribute to rip current pulsations. Although these very low frequency motions can be energetic (J. MacMahan et al., Very low frequency motions on a complex beach, submitted to *Journal of Geophysical Research*, 2003), they are not discussed here.

[5] The focus here is to test two hypotheses for rip current pulsations on a beach with persistent rip channels. The first hypothesis is that the rip current pulsations are due to infragravity motions. *Sonu* [1972] placed one colocated pressure and current meter within the rip channel for a tidal cycle, and found that the rip current pulsations (velocities) were 90° out of phase with the sea surface elevation within the frequency band from 0.004–0.04 Hz (surf beat), consistent with standing infragravity waves (*Suhayda* [1974], *Guza and Thornton* [1985], and others).

[6] The second hypothesis is that the mass transport and wave setup (hydraulic head) produced by the higher waves within wave groups ponds significant amounts of water within the surf zone. During the subsequent minima in the short-wave groups, the ponded water returns outside the surf zone through the rip channels, which are hydraulically more efficient [*Munk*, 1949; *Shepard and Inman*, 1950]. Thus the flow is pumped over the shoal with the incoming short-wave groups and primarily returns through the rip channel.

[7] The two hypotheses can be distinguished by the temporal lag between the maxima of rip current pulsations and the incoming wave groups, and by the alongshore temporal variation of the pulsation, both of which would be large for pulsations driven by ponding and subsequent release of water in the rip channels. The observations

0148-0227/04/2003JC002068$09.00

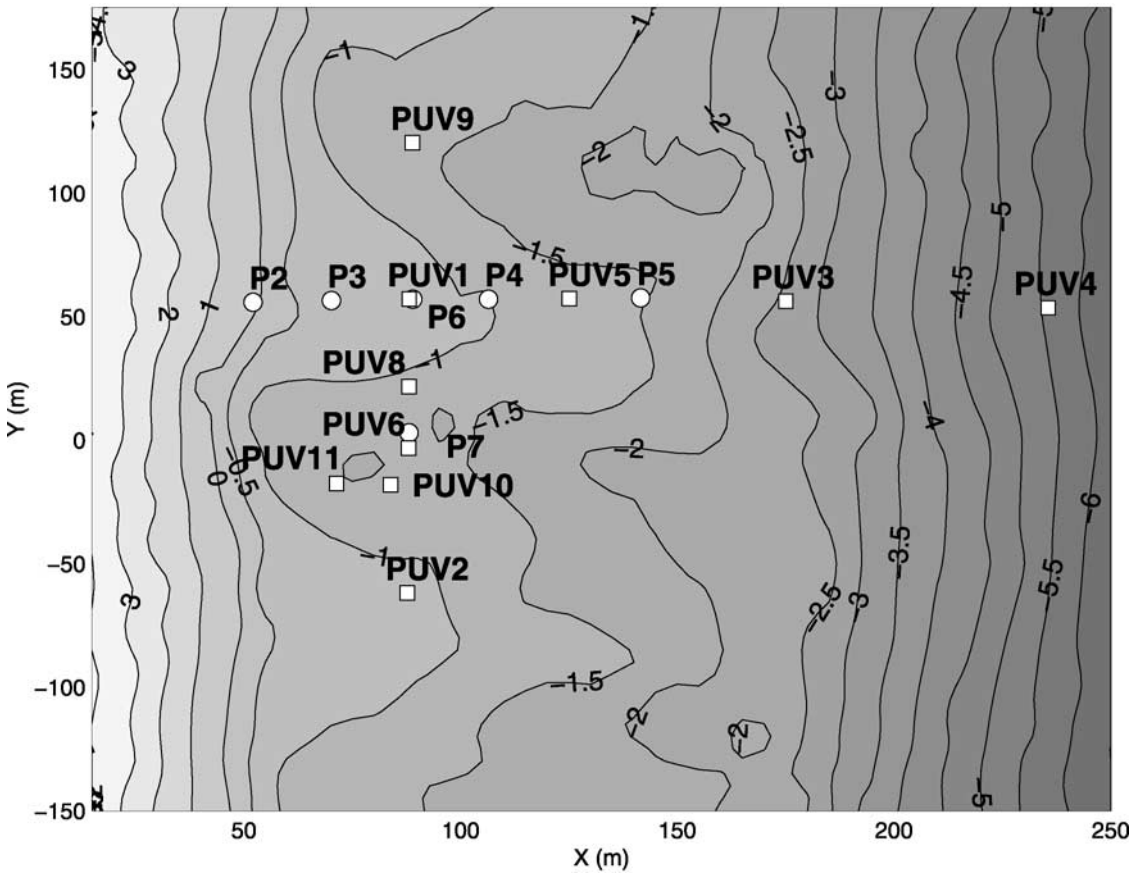

Figure 1. Bathymetry at Sand City, California, for year day 117. The circles are pressure sensors (*P*) and the squares are colocated pressure and bidirectional electromagnetic current meters (PUV).

presented here are consistent with pulsations caused by infragravity motions, but not with ponding by wave groups.

2. RIP Current Field Experiment (RIPEX)–Steep Beach Experiment (SBE)

[8] Observations were obtained on a beach with quasi-periodic rip channels at Sand City, Southern Monterey Bay, California, during the RIP Current Field Experiment (RIPEX)–Steep Beach Experiment (SBE) during the months of April and May 2001. The foreshore of the beach was relatively steep (slope $\sim$0.10) and contained O(35 m) long beach cusps, flattening to a low-tide terrace (slope $\sim$0.01) with incised channels (rip channels) spaced $\simeq$125 m, and continued farther offshore with slope $\sim$0.05 (Figure 1).

[9] An alongshore array of six pressure and bidirectional electromagnetic current meters (PUV) was deployed across the shore-connected shoals and rip channels, and a cross-shore array of pressure (*P*) sensors and PUVs was deployed on the shore-connected shoal (Figure 1). All instruments were sampled continuously and synchronously at 8 Hz. The current meters within the rip channels were oriented downward after year day 117 to obtain measurements during lower tides. Current meters on the shoal were oriented upward, and were not always submerged at low tides.

[10] Offshore waves were measured by a directional wave rider buoy located 650 m offshore in 17 m depth. Considerable variation in both wave height and wave period occurred during the experiment (year day 107–138), with wave direction usually close to normal incidence (Figure 2). The lack of directional variability is associated with the relatively narrow aperture owing to the sheltering effects of the headlands of the bay and strong refraction over Monterey Bay Canyon.

[11] Bathymetric surveys were performed using a differential kinematic global positioning system (KGPS) mounted on a sonar-equipped personal watercraft [*MacMahan*, 2001] at high tide, and mounted in an instrumented backpack carried by a person walking the shore-connected shoals at low tide. Beach face surveys were obtained at low tide with the KGPS mounted on an all terrain vehicle.

[12] The mean flow was predominantly shoreward on the shore-connected shoals and seaward through the rip channels, although there also were mean alongshore currents, resulting in a cellular circulation that was present throughout the experiment, except for low wave conditions. For additional descriptions of the experiment, see J. MacMahan et al. (manuscript in preparation, 2004).

3. Observations of Infragravity Motions

3.1. Cross-Shore and Alongshore Spectral Statistics

[13] Previous observations of rip currents [*Shepard and Inman*, 1950; *Sonu*, 1972; *Aagaard et al.*, 1997; *Brander and Short*, 2001] have documented pulsations on timescales of wave groups, and thus the infragravity motions from

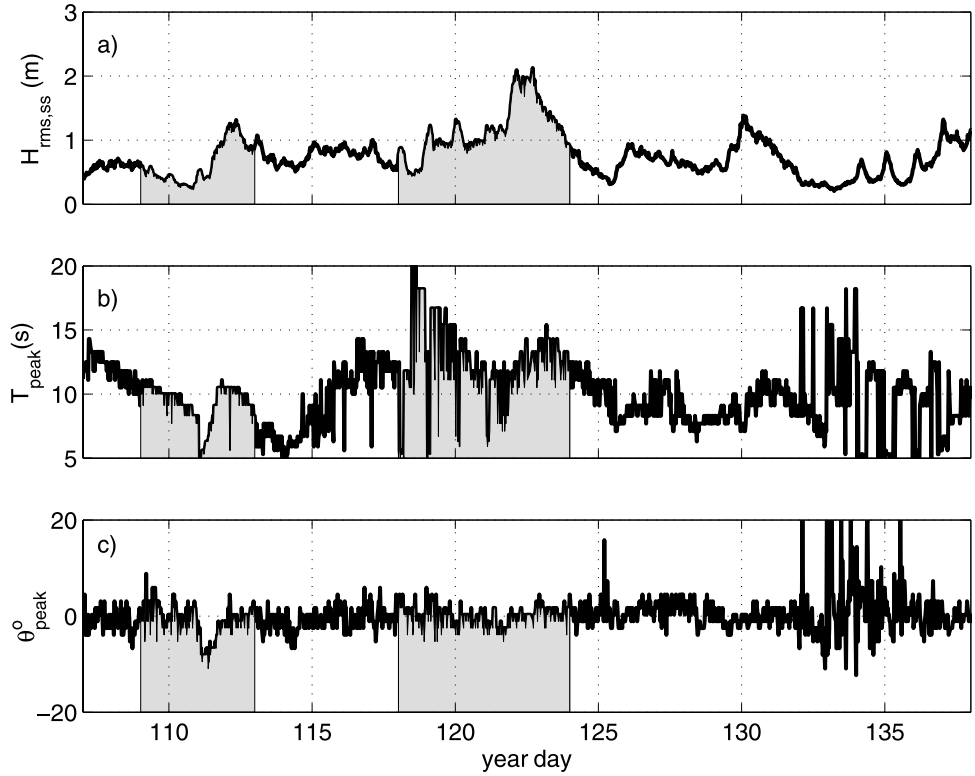

Figure 2. (a) Root-mean-square wave height, $H_{rms,ss}$, within the swell and sea (0.04–0.35 Hz) frequency band (ss); (b) peak wave period, T_{peak}; and (c) peak wave direction, θ_{peak} from a wave-directional buoy in 17 m water depth versus time. Shaded regions represent periods discussed in the text.

outside the surf zone to close to the shoreline are analyzed here. Spectra were estimated from the average of four demeaned, quadratically detrended (to remove tides) 1024 s segments (frequency resolution of 0.001 Hz). Band-passed root-mean-square (rms) values for the sea surface elevation (η_{rms}), cross-shore velocity (u_{rms}), and the alongshore velocity (v_{rms}) were obtained by taking the square root of the integrated energy density spectrum, $E(f)$, within the infragravity, ig, (0.004–0.04 Hz) and within the swell and sea, ss, (0.04–0.35 Hz) frequency bands. Root-mean-squared wave height is defined as $H_{rms} = 2\sqrt{2}\eta_{rms}$.

[14] The local $H_{rms,ss}$ was obtained by transforming the estimated pressure spectra to surface elevation spectra using linear wave theory. For pressure sensors that were buried below the bed, the transformation defined by *Raubenheimer et al.* [1998] was utilized. Average infragravity wave periods were computed using the first spectral moment period, and were approximately 50 ± 5 s for all locations throughout the experiment, varying slightly in the cross shore due to nodal structure (A. J. H. M. Reniers et al., manuscript in preparation, 2004).

[15] The time variation of wave height for both $H_{rms,ss}$ and $H_{rms,ig}$ across the beach profile are presented in Figure 3. The offshore sensor, PUV4, located in 6 m water depth, was well outside of the surf zone, except for the storm that occurred on year day 122 (Figure 3). PUV3, located in 3 m depth, was in the surf zone during storms ($H_{rms,ss} > \sim$1.2 m). P5 (2 m depth), P4 (1.5 m depth), P3 (1 m depth), and P2 (1 m depth) were all on the shore-connected shoal. P5, located on the outer edge of the shoal, sometimes was in the surf zone, whereas P4, P3, and P2 were inside the saturated surf zone, except during times of low wave energy. $H_{rms,ss}$ on the shoal decreases with decreasing depth due to wave breaking, and exhibits a strong tidal modulation, similar to observations by *Thornton and Kim* [1993]. The tidal modulation is more apparent for sensors shoreward of P5.

[16] In contrast to $H_{rms,ss}$, $H_{rms,ig}$ increases with decreasing depth toward the shore (Figure 3). $H_{rms,ig}$ varies minimally with tidal elevation, similar to observations over a barred beach at Duck, North Carolina [*Lippmann et al.*, 1999], but predominantly as a function of the incoming wave energy, consistent with previous observations (*Holman* [1981], *Guza and Thornton* [1985], *Lippmann et al.* [1999], and others).

[17] Pressure sensors (PUV2, P7, PUV8, P6) in the alongshore array (Figure 1) were operational for 5 days (year days 109–114). Therefore analysis of the alongshore infragravity motions focuses on the cross-shore and alongshore velocities. The $u_{rms,ig}$ was greater than $v_{rms,ig}$ and exhibited a small amount of tidal modulation (Figure 4). The tidal modulation of $u_{rms,ig}$ and $v_{rms,ig}$ results from tidal variations in depth, consistent with the long-wave relationship ignoring bottom slope effects, given by

$$U_{rms,ig} = \eta_{rms,ig}\sqrt{\frac{g}{h}}, \tag{1}$$

where $U_{rms,ig}$ is $\sqrt{u^2_{rms,ig} + v^2_{rms,ig}}$, g is the gravitational acceleration, and h is the local water depth [*Dean and*

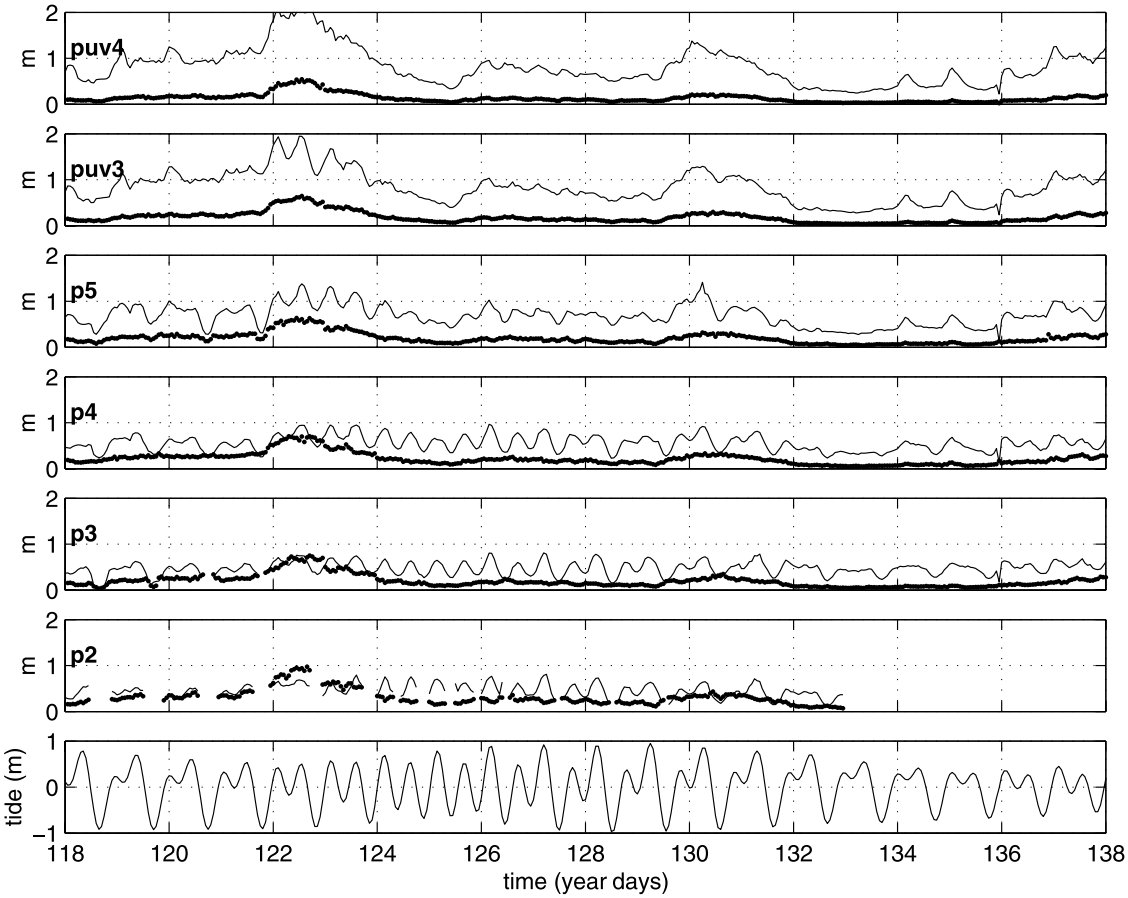

Figure 3. H_{rms} along the cross-shore transect versus time. Thick curves are $H_{rms,ig}$, and thin curves are $H_{rms,ss}$. Sensors are labeled in each panel, and tidal level is shown at the bottom.

Dalrymple, 1984]. Equation (1) was evaluated using hourly statistics at PUV2, 5, 11 located on the shore-connected shoal and within the rip channel, when both the current meter and pressure sensors were operational. The measurements are consistent with equation (1), with r^2 values of 0.87, 0.88, and 0.93 and slopes, m, of 0.71, 0.83, and 0.79 for the three locations. The relationship is biased low (i.e., $m < 1$) for all three locations, suggesting that there are no additional contributions to low frequency motions.

[18] Total infragravity velocity magnitudes ($U_{rms,\ ig}$) were computed for year days 117–124, when there was minimal alongshore profile change (Figure 5). The relatively large alongshore differences in the $U_{rms,ig}$ are statistically significant with the 95% confidence interval. The $U_{rms,ig}$ variations are associated with alongshore differences in bathymetric elevations (Figure 5), owing to the infragravity velocities dependence on depth ($h^{-1/2}$ (equation (1)). Thus the magnitude of the $U_{rms,ig}$ is smaller within the rip channel.

3.2. F-k_y Spectral Estimates

[19] Frequency–wave number spectra, $S(f, k_y)$, were estimated from cross-shore and alongshore velocities for the alongshore array using the iterative maximum likelihood estimator (IMLE) [*Pawka*, 1983; *Oltman-Shay and Guza*, 1987]. Infragravity motions of u and v are relatively homogenous in alongshore space, and thus it is assumed that the alongshore lag array can be used to estimate the $S(f, k_y)$ spectra to discriminate modes of edge and leaky waves [*Huntley et al.*, 1981; *Oltman-Shay and Guza*, 1987; A. J. H. M. Reniers et al., manuscript in preparation, 2004]. Owing to different instrument locations, each cross-spectral value was normalized such that the diagonals of the cross-spectral matrix are unity. Spectral estimates with 64 degrees of freedom (frequency resolution of 0.002 Hz) were generated from demeaned, quadratically detrended 4.55 hour records.

[20] Frequency–wave number spectra were computed for year days 107–138, and the spectral energy integrated over the infragravity frequency bands (Figure 6). Most of the infragravity energy is confined to cross-shore velocities centered near $k_y = 0\ m^{-1}$, indicating the dominance of cross-shore infragravity waves, consistent with narrowband incident waves [*Oltman-Shay et al.*, 1989; *Herbers et al.*, 1995], except during storm events (e.g., year day 122 in Figure 6).

[21] If the rip current pulsations within the infragravity band were caused by ponding and subsequent release of water through the rip channels, such that there was a time difference between incoming flow over the shore-connected shoal and the return flow through the rip channels, energy would be found along $k_y = \pm 0.008\ m^{-1}$ (Figure 6), which are associated with the rip channel

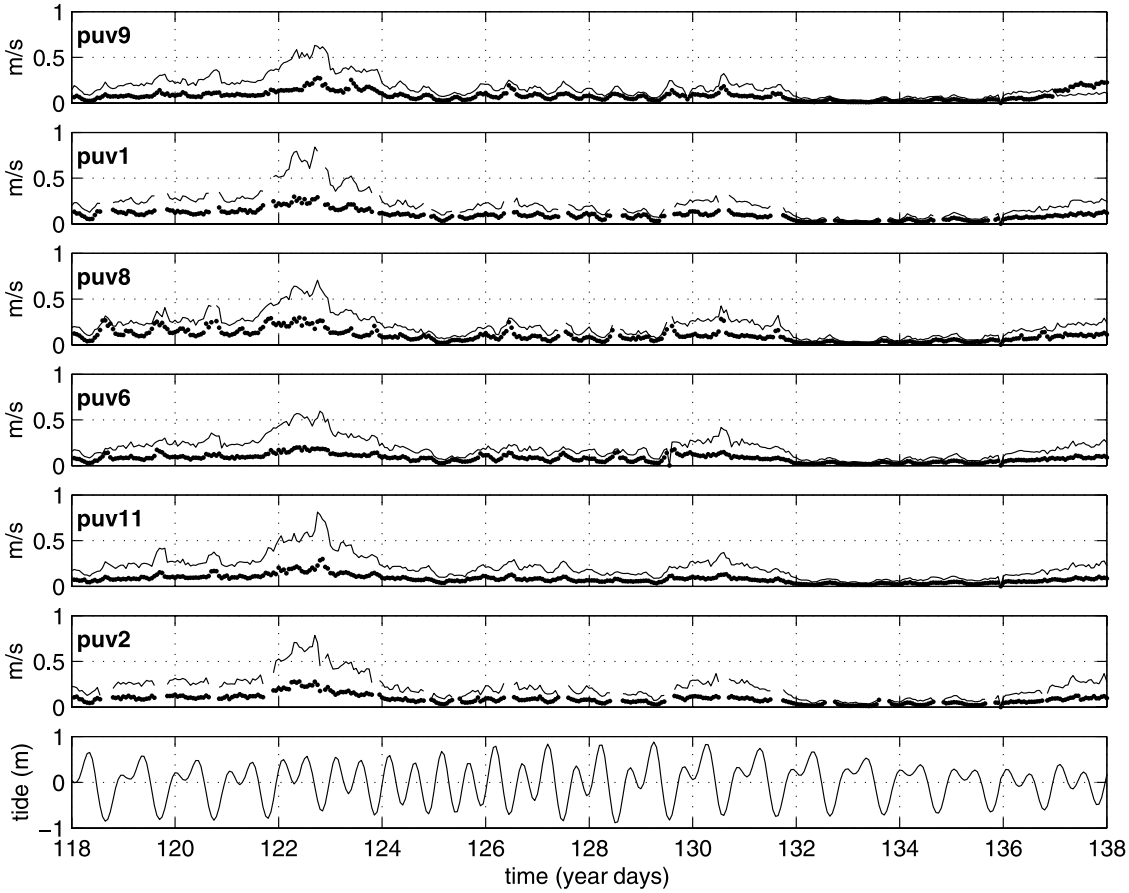

Figure 4. Infragravity velocities along the alongshore array versus time. Thick curves are $v_{rms,ig}$, and thin curves are $u_{rms,ig}$. Sensors are labeled in each panel, and tidal level is shown at the bottom.

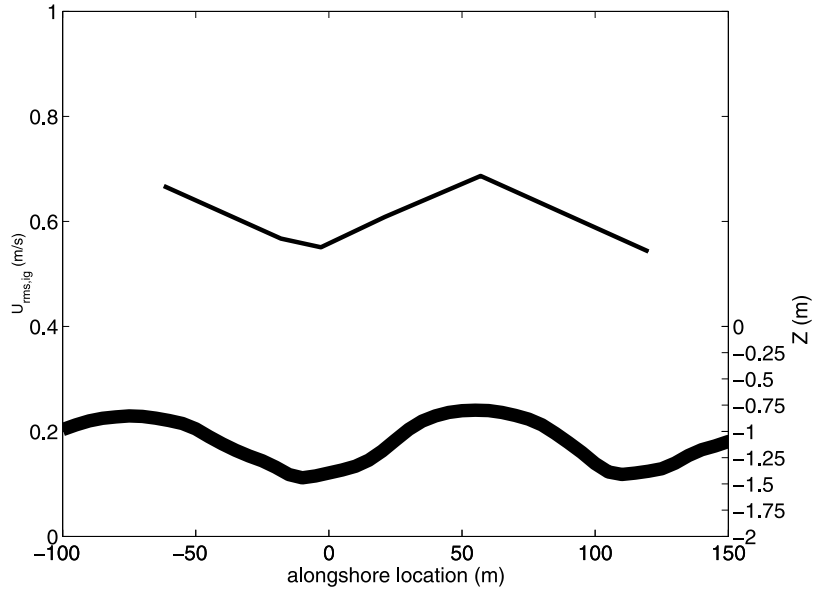

Figure 5. $U_{rms,ig}$ for year days 117–124 within the alongshore array. The 95% confidence interval is represented by the thickness of the $U_{rms,ig}$ curve. The corresponding alongshore water depth is shown as a thick curve (depth is labeled on the right-hand side).

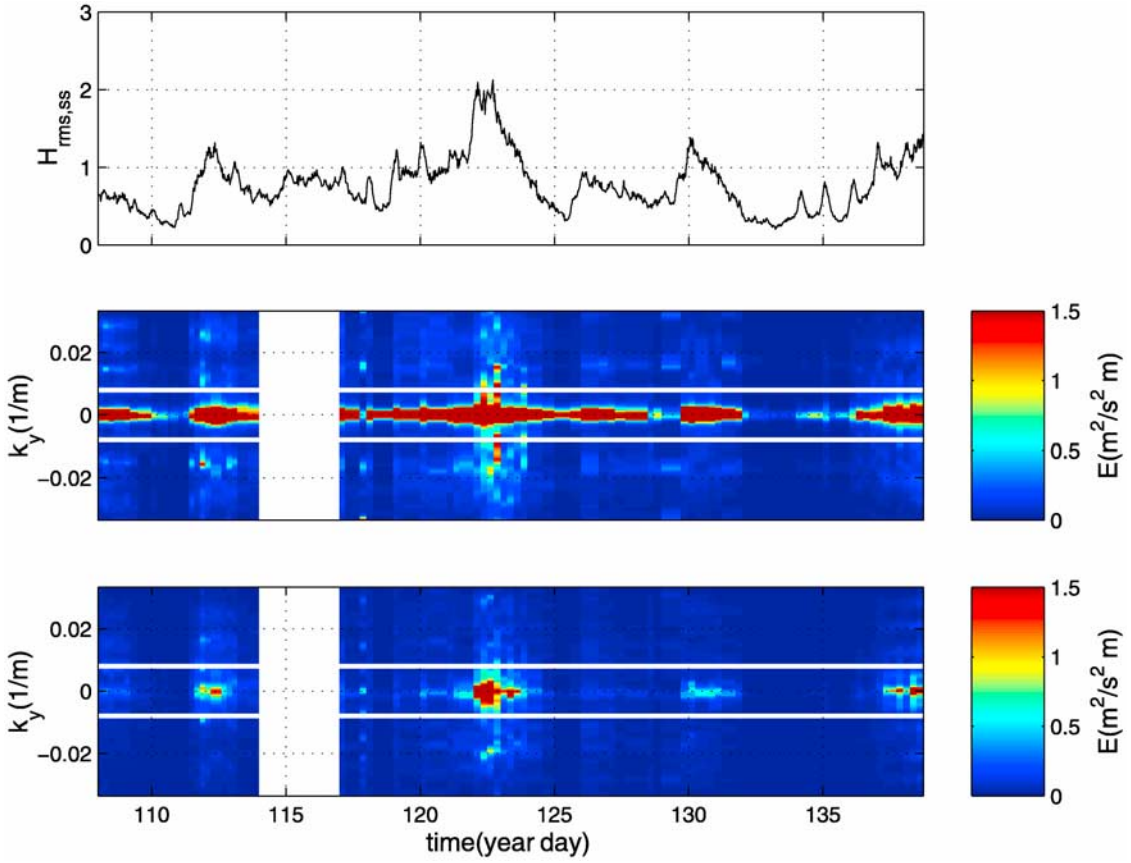

Figure 6. (top) $H_{\mathrm{rms,ss}}$ measured at the buoy versus time. Contours (color scale on the right) of integrated energy within the infragravity frequency band for (middle) cross-shore and (bottom) alongshore velocities in the alongshore array as a function of alongshore wave number (k_y) and time. The white lines represent the rip channel spacing at $k_y = \pm 0.008$ m^{-1}. White blocks indicate times when the current meters were not operational.

spacings. This is not the case, suggesting another mechanism causes the pulsations.

4. Rip Current Pulsations

4.1. Alongshore Temporal Structure of Infragravity Velocities and Pressure

[22] The cross correlations ($R(\tau)$) between observations on the alongshore transect are high at zero time lag (τ). The high correlations at zero time lag for cross-shore infragravity velocities (Figure 7a), suggests that the infragravity waves respond similarly in time across the shore-connected shoal and the rip channels, and temporally are unaffected by the presence of the alongshore varying bathymetry. The alongshore array may not be parallel to the shoreline, so the time lag for the maximum cross correlation for the cross-shore velocities was computed. The absolute maximum time difference between sensors is approximately 5 s at midtide (Figure 7b) suggesting minimal array orientation bias with PUV9, located around $y = 120$ m, appearing to be slightly closer to the shoreline. During lower tidal elevations (Figure 7e), but when the current meters were submerged, the temporal correlation value decreased, but still remained relatively high (Figures 7a and 7b).

[23] The period of record for Figure 7, representative of the entire experiment, was chosen because four of the seven pressure sensors in the alongshore array were operational. The four operational pressure sensors (PUV2, P7, PUV8, and P6) span the rip channel ($y = -20$ m), north of the cross-shore array. Unlike the current meters, the pressure sensors were submerged throughout the tidal cycle. At $\tau = 0$, infragravity frequency sea surface elevation fluctuations are correlated both on the shoal and within the rip channel (Figure 7c). Similar to the alongshore correlations of velocity, the correlation decreases with lower tidal elevation (Figure 7e). The correlation is zero at extremely low tides, which corresponds to periods when the shore-connected shoal is barely submerged. The time lag for the maximum correlation is zero (Figure 7d), except for the lowest tidal elevations for which it is approximately 10 s. This time lag occurred when the shore-connected shoal was barely submerged while the rip channel was covered by approximately 1 m of water.

[24] The theoretical time lag ($\triangle t$) for a long wave to propagate over a sloping bed between the two locations ($\triangle x$) is given by

$$\triangle t = \int_{\triangle x} \frac{dx}{d[\sqrt{gh}]}. \tag{2}$$

The long-wave propagation speed ($\sqrt{gh}$) is retarded over the shallower water depths of the shore-connected shoal.

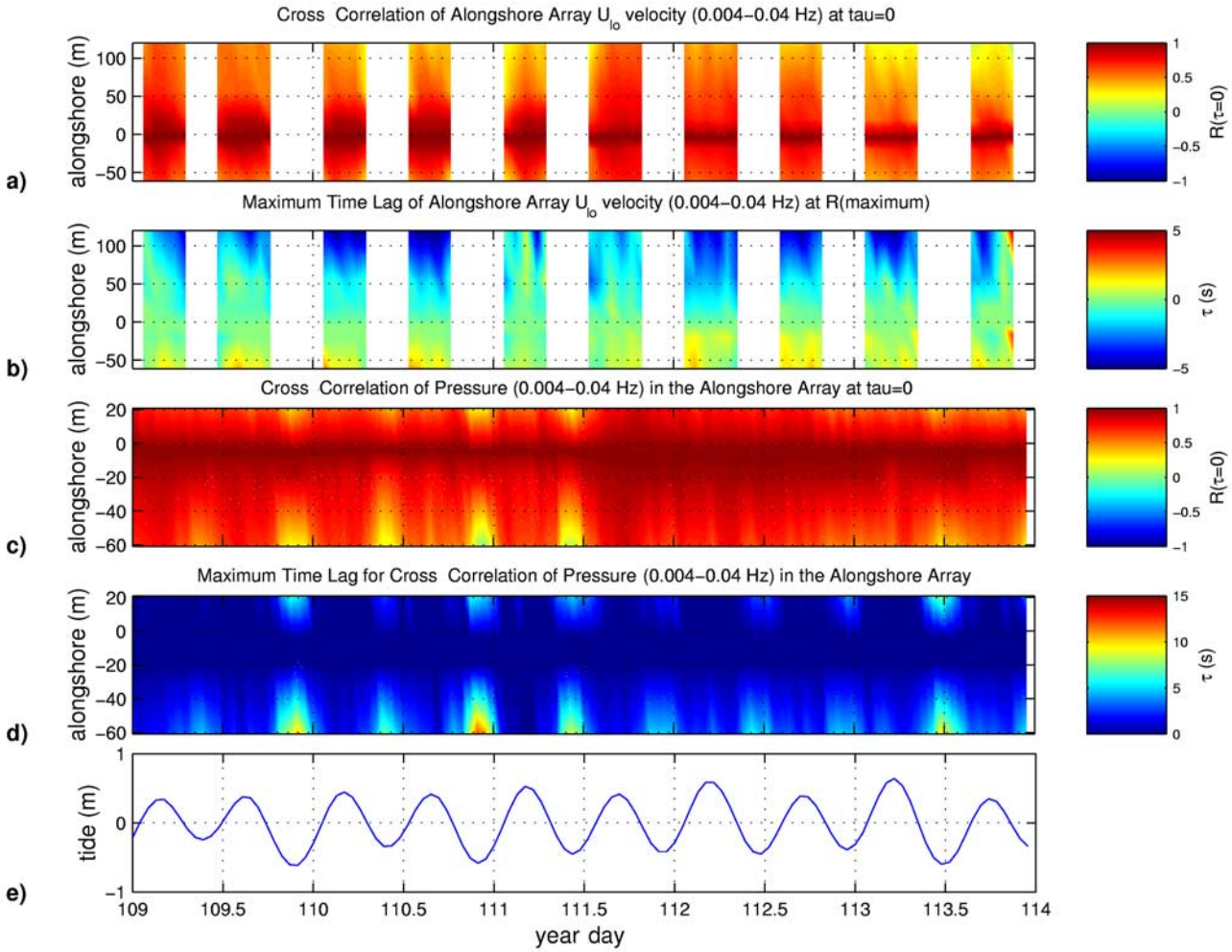

Figure 7. (a) Contours (color scales at the right) of cross correlations at zero time lag between cross-shore velocities in the alongshore array; (b) the time lag of the maximum correlation for the cross-shore velocities in the alongshore array; (c) cross correlations at zero time lag for pressure in the alongshore array; and (d) the time lag of the maximum correlation for the pressure in the alongshore array as a function of alongshore location and time. (e) Tidal elevation versus time. White blocks indicate times when the current meters were not submerged.

The observed 10*s* time lag (Figure 6d) is consistent with the theoretical time difference (9 s) (equation (2)) between a long wave propagating from PUV4 to P6 (on the shoal) and to P7 (within the rip channel). These results indicate that the bathymetry has minimal temporal effects on the infragravity motions, except during low tides, and that the cross-shore infragravity motions primarily are responsible for the rip current pulsations at these frequencies.

4.2. Cross Correlation Functions of Infragravity Motions With Rip Current Pulsations

[25] Cross correlation functions of rip current pulsations, wave groups, and infragravity sea surface elevations were evaluated to determine the temporal characteristics associated with the rip current pulsations and infragravity forcing mechanisms. The wave amplitude envelope, $A(t)$, is obtained by low-pass filtering (cut-off frequency is 0.04 Hz) the absolute value of the Hilbert transform of sea surface elevation within the 0.004–0.04 Hz frequency band [*Melville*, 1983]. The short-wave group energy, $E(t)$, is calculated from the short-wave envelope, $A(t)$, as

$$E(t) = \frac{1}{2}\rho g A(t)^2, \tag{3}$$

where ρ is the density of seawater. PUV11 (after year day 117 when the current meters were inverted) is utilized because it was located within the rip channel along the alongshore array, and both current and pressure sensors were operational throughout the experiment.

[26] The cross correlation between infragravity elevation and cross-shore velocity at PUV11 is zero at zero time lag (Figure 8a), with maximum correlations occurring at approximately 15 s lag. This relationship is indicative of a standing wave, for which elevation and velocity are in quadrature. If the sensors were located at a spatial node or antinode, correlation would be zero for all time lags, which is not the case. The correlation is negative at approximately −15 s time lag and positive at ∼15 s time

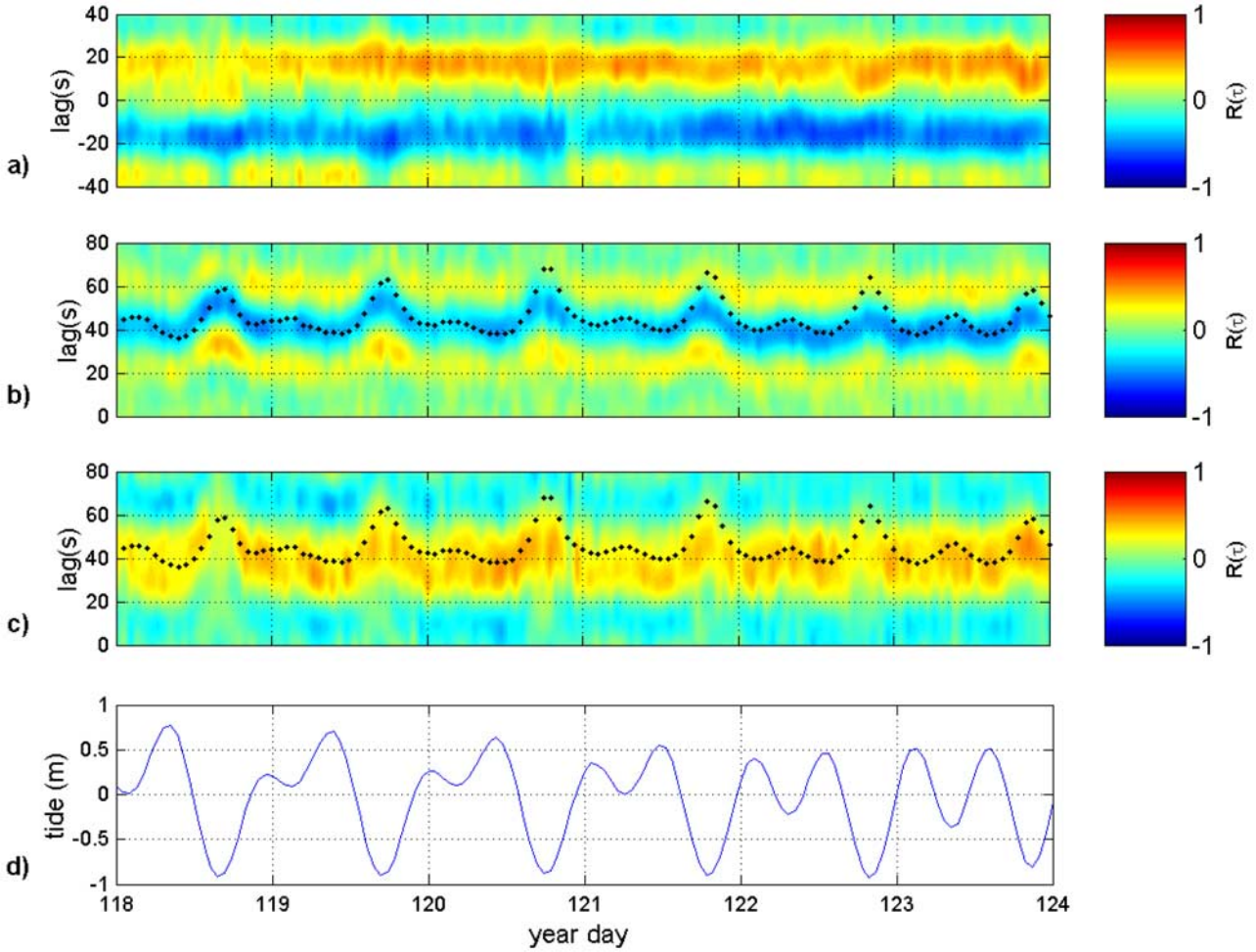

Figure 8. Contours (color scale at the right) of cross-correlation functions for (a) rip channel infragravity elevation (PUV11) and rip channel cross-shore infragravity velocity (PUV11); (b) offshore wave group energy (PUV4) and rip channel cross-shore infragravity velocity (PUV11); and (c) offshore infragravity elevation (PUV4) and rip channel infragravity elevation (PUV11) as a function of lag and time. The theoretical time lag for long-wave propagation is shown as a dotted curve (equation (2)). (d) Tidal elevation versus time.

lag, corresponding to approximately half of the infragravity wave period. If the infragravity waves were progressive, a maximum correlation between elevation and cross-shore velocity would occur at zero time lag.

[27] The offshore wave group energy (PUV4) and the nearshore infragravity cross-shore velocity (rip current pulsation) (PUV11) are negatively correlated at the theoretical time lag (equation (2)) (Figure 8b), consistent with an infragravity bound long wave traveling 180° out of phase with the wave group energy. Thus the maximum offshore velocity occurs at the maximum of the short-wave group, not during the subsequent minimum, when the ponded water would be released. Note that the positive correlation centered around T = 20 s is associated with a preceding free infragravity wave (A. J. H. M. Reniers et al., manuscript in preparation, 2004), whereas the positive correlation centered around T = 60 s is associated with the reflection at the shoreline of the incoming bound infragravity wave. The positive cross correlations between the offshore infragravity elevation (PUV4) and the rip channel infragravity elevation (PUV11) are consistent with theory (Figure 8c), suggesting that the theoretical time lag utilized in Figure 8b is appropriate.

[28] The correlation functions (Figures 8a–8c) do not change greatly during the 8 day observational period, except for tidal variations owing to differences in propagation speeds. The results indicate that the short-wave group and long-wave evolution over the shoal are related to the cross-shore motions of the infragravity waves. Thus the observed rip current pulsations within the infragravity frequency band are consistent with forcing by standing infragravity waves.

5. Conclusions

[29] Two hypotheses have been proposed for the forcing of rip current pulsations in the infragravity frequency band. One hypothesis is that the rip current pulsations are due to infragravity standing waves [*Sonu*, 1972]. The second hypothesis is that there is a maximum of setup within the

surf zone when the largest short waves in a wave group break, resulting in a transport of water shoreward that is discharged most efficiently through the rip channels during the subsequent small short waves of the wave group [*Munk*, 1949; *Shepard and Inman*, 1950].

[30] The measurements reported here are consistent with the first hypothesis, and do not support the second hypothesis. Specifically, the alongshore variations in velocities and sea surface elevations can be explained by the depth difference between rip channels and neighboring shoals, and are inconsistent with ponding of water by incoming short waves that subsequently is released within the rip channels. In contrast, consistent with previous studies, the observations suggest cross-shore standing waves are the primary forcing of infragravity frequency pulsations of the rip currents on this beach.

[31] **Acknowledgments.** We thank Tom Herbers and Paul Jessen for providing offshore buoy data. We extend our appreciation to the many folks who assisted in obtaining a great data set: Loraine Chial, Ron Cowen, Jason Engle, Tom Lippmann, James Joyner, Gregory Miller, Denis Morichon, Bruce Morris, Mark Orzech, Jennifer Short, Sidney Schofield, Jim Stockel, Charlotte Webb, Rob Wyland, volunteers from Hopkins Marine Station (Stanford University) led by Mark Denny, and a special thanks to Edie Gallagher for the instrument surveys. The Steep Beach Experiment was funded by the Office of Naval Research, Coastal Sciences Program, under contract N0001402WR20188 and data analysis by ONR and the National Science Foundation under contract OCE-01366882. J.M. was funded by the Florida Sea Grant Program and the National Science Foundation under contract OCE-01366882. A.R. held a National Research Council–NPS Research Associateship funded by ONR and NSF. We thank Steve Elgar and an anonymous reviewer for their critical, but valuable, comments, making this a better paper.

References

Aagaard, T., B. Greenwood, and J. Nielsen (1997), Mean currents and sediment transport in a rip channel, *Mar. Geol.*, *140*, 24–45.

Brander, R. W., and A. D. Short (2001), Flow kinematics of low-energy rip current systems, *J. Coastal Res.*, *17*(2), 468–481.

Dean, R. G., and R. A. Dalrymple (1984), *Water Wave Mechanics for Engineers and Scientists*, Prentice-Hall, Old Tappan, N. J.

Guza, R. T., and E. B. Thornton (1985), Observations of surf beat, *J. Geophys. Res.*, *90*, 3161–3171.

Haller, M. C., and R. A. Dalrymple (2001), Rip current instabilities, *J. Fluid Mech.*, *433*, 161–192.

Herbers, T. H. C., S. Elgar, and R. T. Guza (1995), Generation and propagation of infragravity waves, *J. Geophys. Res.*, *100*, 24,863–24,872.

Holman, R. A. (1981), Infragravity energy in the surf zone, *J. Geophys. Res.*, *86*, 6442–6450.

Huntley, D. A., R. T. Guza, and E. B. Thornton (1981), Field observations of surf beat: 1. Progressive edge waves, *J. Geophys. Res.*, *86*, 6451–6466.

Lippmann, T. C., T. H. C. Herbers, and E. B. Thornton (1999), Gravity and shear wave contributions to nearshore infragravity motions, *J. Phys. Oceanogr.*, *29*, 231–239.

MacMahan, J. (2001), Hydrographic surveying from a personal watercraft, *J. Surv. Eng.*, *127*(1), 12–24.

Melville, W. K. (1983), Wave modulation and breakdown, *J. Fluid Mech.*, *128*, 489–506.

Munk, W. H. (1949), Surf beats, *Eos Trans. AGU*, *30*(6), 849–854.

Oltman-Shay, J., and R. T. Guza (1987), Infragravity edge wave observations on two California beaches, *J. Phys. Oceanogr.*, *17*, 644–663.

Oltman-Shay, J., P. A. Howd, and W. A. Birkemeier (1989), Shear instabilities of the mean longshore current: 2. Field observations, *J. Geophys. Res.*, *94*, 18,031–18,042.

Pawka, S. S. (1983), Island shadows in wave directional spectra, *J. Geophys. Res.*, *88*, 2579–2591.

Raubenheimer, B., S. Elgar, and R. T. Guza (1998), Estimating wave heights from pressure measured in the sand bed, *J. Waterw. Port Coastal Ocean Eng.*, *124*(3), 151–154.

Reniers, A. J. H. M., J. A. Roelvink, and E. B. Thornton (2004), Morphodynamic modeling of an embayed beach under wave group forcing, *J. Geophys. Res.*, *109*, doi:10.1029/2002JC001586, in press.

Shepard, F. P., and D. L. Inman (1950), Nearshore water circulation related to bottom topography and wave refraction, *Eos Trans. AGU*, *31*(2), 196–212.

Shepard, F. P., K. O. Emery, and E. C. La Fond (1941), Rip currents: A process of geological importance, *J. Geol.*, *49*, 337–369.

Smith, J. A., and J. L. Largier (1995), Observations of nearshore circulation: Rip currents, *J. Geophys. Res.*, *100*, 10,967–10,975.

Sonu, C. J. (1972), Field observation of nearshore circulation and meandering currents, *J. Geophys. Res.*, *77*, 3232–3247.

Suhayda, J. N. (1974), Standing waves on beaches, *J. Geophys. Res.*, *79*, 3065–3071.

Thornton, E. B., and C. S. Kim (1993), Longshore current and wave height modulation at tidal frequency inside the surf zone, *J. Geophys. Res.*, *98*, 16,509–16,520.

J. H. MacMahan, T. P. Stanton, and E. B. Thornton, Oceanography Department, Code OC/Tm, Naval Postgraduate School, Monterey, CA 93943, USA. (jhmacmah@nps.navy.mil; stanton@oc.nps.navy.mil; ebthornt@nps.navy.mil)

A. J. H. M. Reniers, Civil Engineering and Geosciences, Delft University of Technology, Stevinweg 1, Delft ZH 2628CN, Netherlands. (ad@dutcvmm.ct.tudelft.nl)